Eur. Phys. J. D (2017) 71: 130
DOI: 10.1140/epjd/e2017-70709-6

THE EUROPEAN PHYSICAL JOURNAL D

Regular Article

# Monte Carlo simulation of proton track structure in biological matter*

Michele A. Quinto[1], Juan M. Monti[1], Philippe F. Weck[2], Omar A. Fojón[1], Jocelyn Hanssen[1], Roberto D. Rivarola[1], Philippe Senot[3], and Christophe Champion[4,a]

[1] Instituto de Física Rosario, CONICET – Universidad Nacional de Rosario, S2000 EKF Rosario, Argentina
[2] Sandia National Laboratories, Albuquerque, NM, USA
[3] Université de Lorraine, CNRS, Institut de Chimie, Physique et Matériaux, 57 000 Metz, France
[4] Université de Bordeaux, CNRS/IN2P3, Centre d'Etudes Nucléaires de Bordeaux Gradignan, CENBG, 33170 Gradignan, France

Received 12 November 2016 / Received in final form 9 February 2017
Published online 25 May 2017 – 

**Abstract.** Understanding the radiation-induced effects at the cellular and subcellular levels remains crucial for predicting the evolution of irradiated biological matter. In this context, Monte Carlo track-structure simulations have rapidly emerged among the most suitable and powerful tools. However, most existing Monte Carlo track-structure codes rely heavily on the use of semi-empirical cross sections as well as water as a surrogate for biological matter. In the current work, we report on the up-to-date version of our homemade Monte Carlo code *TILDA-V* – devoted to the modeling of the slowing-down of 10 keV–100 MeV protons in both water and DNA – where the main collisional processes are described by means of an extensive set of ab initio differential and total cross sections.

## 1 Introduction

Whether it is in radiobiology to identify the DNA critical lesions or in medicine to adapt the radio-therapeutic protocols, a detailed understanding of the radio-induced interactions in living matter is required. In this context, numerical simulations based on Monte Carlo (MC) approach are among the most suitable and powerful tools with a large spectrum of applications in numerous fields.

Among existing MC codes (see the review by Nikjoo et al. [1]), some of them – known as condensed-history codes – are based on a macroscopic description of the particle transport (multiple scattering theory) and mainly developed for general-purpose applications. However, within the scope of micro-dosimetry, those MC codes appear limited and inadequate to predict the radio-induced energy deposits at the *nanoscale* level. Because of those shortcomings, condensed-history codes are generally supplanted by MC *track-structure* (MCTS) approaches, where the full particle histories are described step-by-step, interaction after interaction, for both the incident beam and the secondary particles potentially created. The development of such event-by-event MCTS codes has been notably slower than for condensed-history codes, since it involves collecting or generating large sets of input data (cross sections) needed to describe the various particle-induced interactions at the atomic scale in the medium of interest (e.g., water and DNA). In general, MCTS codes devoted to the charged particle track modeling in biological matter include input databases taken from different standards (see for example [2–5]), mainly based on experimental data and/or semi-empirical approaches. Moreover, it is worth noting that the vast majority of existing numerical codes to model proton-induced damage and its derivatives (radiotherapy, dosimetry, medical imaging, etc.) uses water as tissue-equivalent medium with – for the most sophisticated – the modeling of the chemical species and the free radical creation and diffusion to estimate the *indirect* radiation effect on DNA and/or the inclusion of the molecular DNA structure, the latter being generally superimposed on the ion track-structure in water (see for example Ref. [6]).

In the current work, we aim at going beyond the use of water as a surrogate for the biological medium, and reporting on the newly developed track-structure code *TILDA-V* (an acronym for "Transport d'Ions Lourds Dans l'Aqua & Vivo" [7]) which refers to an extension of the *TILDA* Monte Carlo code previously developed by Champion et al. [8] for modeling heavy ion and secondary electron histories in liquid and gaseous water for impact energies ranging from 10 keV/u to 100 MeV/u. The present version is based on an extensive set of ab initio multiple differential and total cross sections for describing the main inelastic processes occurring during the slowing-down of protons in water and DNA components (adenine

* Contribution to the Topical Issue "Many Particle Spectroscopy of Atoms, Molecules, Clusters and Surfaces", edited by A.N. Grum-Grzhimailo, E.V. Gryzlova, Yu V. Popov, and A.V. Solov'yov.

[a] e-mail: champion@cenbg.in2p3.fr

(A), thymine (T), cytosine (C), guanine (G) and sugar phosphate (SP) backbone). Nevertheless, let us add that some collisional processes are still *semi-empirically* considered in the up-to-date version, namely, via existing analytical fits based on the most recent experiments, in particular for the excitation process, whose modelling is actually in progress.

To the best of our knowledge, *TILDA-V* is the first MC track-structure code able to simulate the full transport of protons and its secondaries in a "realistic" biological medium. Comparisons with existing MCTS code predictions in terms of electronic stopping power are provided in this study.

## 2 The TILDA-V code

### 2.1 Charged particle transport

Monte Carlo charged particle transport simulation comprises series of sampling steps, which first determine the distance $\lambda$ between two successive interactions. The latter is selected by assuming that the charged particle transport in matter is governed by a Poisson law $p(\lambda)$, whose corresponding probability $P(\lambda)$ is defined by

$$P(\lambda) = \int_0^{\lambda} p(u)du = 1 - \exp\left(\frac{-\lambda}{\bar{\lambda}}\right). \quad (1)$$

This probability is usually sampled by means of pseudo-random variables defined in the interval [0;1], namely, $\Gamma \equiv \Gamma(0;1)$, that finally leads to a distance $\lambda$ given by

$$\lambda = -\bar{\lambda}\ln(1-\Gamma) = -\bar{\lambda}\ln(\Gamma') \quad \text{with} \quad \Gamma' \equiv \Gamma'(0;1). \quad (2)$$

In equation (1), $\bar{\lambda}$ refers to the mean free path defined as $\bar{\lambda} = 1/(n\sigma_T)$, where $n$ denotes the number of target molecules per volume unit defined as $n = N_A * \rho/A_{mol}$, where $N_A$ is the Avogadro's number, $\rho$ and $A_{mol}$ are the density (in g cm$^{-3}$) and the molar mass of the crossed medium, respectively, and $\sigma_T$ is the total cross section including all the interactions considered for modelling the transport of the particle of interest.

In its current version, *TILDA-V* takes into account the following collisional processes:

- for protons: elastic scattering, ionization, capture and excitation;
- for neutral-hydrogen atoms: elastic scattering, ionization, capture, electron loss (stripping) and excitation;
- for secondary electrons: elastic scattering, ionization and excitation.

The second sampling refers to the collision type that occurs at the selected position. Whether it is for primary protons or secondary electrons, the latter is randomly chosen according to the relative magnitude of the individual total cross section of each collisional process (elastic as well as inelastic). The collision type $k$ is simply given by

$$\sum_{i=1}^{k-1} P_i \leqslant \Gamma \leqslant \sum_{i=1}^{k} P_i \quad \text{with} \quad P_i = \frac{\sigma_i}{\sigma_T}. \quad (3)$$

If the selected interaction is ionizing, a third sampling procedure is performed in order to select the molecular subshell impacted by considering the contribution of each target subshell to the total cross section of the selected process, namely, by using the *partial* cross sections. Finally, random samplings are performed in order to quantify the full kinematics of the selected interaction. This step is obviously the most time consuming since it requires parsing in a large database (>10 Gb memory size) needed for describing the numerous collisional processes cited above. Let us add that these input data represent a large amount of stored information that are precalculated, namely, within a logarithmic grid of incident proton energies $E_{inc}$ (ranging from 10 keV to 100 MeV), for predefined values of ejected electron energy logarithmically ranging from a minimal value of 0.1 eV to a maximal value $E_e^{max} = 4\frac{m_0}{M_p}E_{inc}$ (where $M_p$ and $m_0$ refer to the proton and the electron mass, respectively) as well as within a linear grid of polar angles ($\theta_e$, $\theta_s$) ranging from 0 to 180°. All these data are stored by way of tables in which kinematical parameters are put in correspondence to their respective differential cross sections.

Once the collision type is defined, the incident proton energy is reduced by the total energy transfer, which includes both the kinetic energy given to the secondary electron potentially created and the potential energy (binding energy, excitation energy, etc.) assumed as locally deposited. The charge state of the primary proton may also change according to the selected collision. Thus, the electron capture will decrease the initial proton charge (from +1 to 0), whereas the electron loss process (stripping) will increase the hydrogen charge (from 0 to +1). The formation of $H^-$ may also occur when the hydrogen atom captures an electron. However, due to the low magnitude of the hydrogen-induced capture cross section (see Ref. [9]), we have neglected this channel in the current version of *TILDA-V*.

The full tracking of all the secondary electrons created along the various proton/hydrogen-induced collisions is carried out by means of the above-cited set of multiple differential and total cross sections to characterize the ejection and scattering spectra along the electron-induced collisions.

Those steps are repeated for all primary and secondary particles until their kinetic energy falls below a predetermined cut-off value. For the primary particles, namely, protons and neutral-hydrogen atoms, the energy cut-off is fixed at 10 keV, while the secondary electrons are followed down to 7.34 eV, i.e. the excitation threshold of the water molecule [10]. Sub-threshold primary ion-projectiles as well as secondary electrons are not followed and assumed as locally absorbed by the medium. The residual energy of such "dead particles" is deposited in a single step at a single point. Then, to assume that these slow particles stay where they originated, introduces uncertainties in the map of the energy deposits scored at the end of the physical stage following the irradiation ($t < 10^{-15}$ s). These latter are smaller or of the order of the projected range $R$ of the corresponding energy

particle, namely, $R(10\ \text{keV}) \cong 0.4\ \mu\text{m}$ for protons [3] and $R(7.34\ \text{eV}) \cong 1\ \text{nm}$ for electrons [11]. From a practical point of view, the computational time needed for simulating the full track of 1 million proton histories ranges from a few hours for the less energetic ones (10 keV) to a few days for 100 MeV protons.

Additionally, let us add that in the case of target inner-shell ionization, the vacancy may be accompanied by non-radiative transitions including the emission of Auger as well as Coster-Krönig electrons that takes place at a short time scale after the interaction, typically between 0.001 and 5 fs. These various processes have been included in *TILDA-V* for all the targets investigated, namely, by considering the probability and the corresponding electron energy. For water, we used the data reported in Martin's thesis [12], while for DNA we used the Auger electron non-radiative probabilities and energies provided by the Livermore Evaluate Atomic Data Library [13] for the different atomic constituents involved in the biomolecular target description. A summary of the data needed is given in Table 1.

**Table 1.** Probabilities and corresponding energy transfers for the non-radiative transitions taken into account in *TILDA-V* for water and DNA.

| Water | | | | |
|---|---|---|---|---|
| *Subshells* | | | *Probability* | *Energy (eV)* |
| $1a_1$ | $2a_1$ | $2a_1$ | 0.0994 | 478.82 |
| $1a_1$ | $2a_1$ | $1b_2$ | 0.0994 | 493.86 |
| $1a_1$ | $2a_1$ | $3a_1$ | 0.1988 | 493.90 |
| $1a_1$ | $2a_1$ | $1b_1$ | 0.1988 | 493.90 |
| $1a_1$ | $1b_2$ | $1b_2$ | 0.1988 | 508.90 |
| $1a_1$ | $1b_2$ | $3a_1$ | 0.1988 | 508.90 |
| $1a_1$ | $1b_2$ | $1b_1$ | 0.1988 | 508.94 |
| $1a_1$ | $3a_1$ | $3a_1$ | 0.1988 | 508.94 |
| $1a_1$ | $3a_1$ | $1b_1$ | 0.1988 | 508.98 |
| $1a_1$ | $1b_1$ | $1b_1$ | 0.1988 | 508.98 |
| Atomic components of the various biomolecules included in the DNA description | | | | |
| Carbon | | | | |
| *Subshells* | | | *Probability* | *Energy (eV)* |
| K | L1 | L1 | 4.13609E-01 | 255.890 |
| K | L1 | L2 | 1.36190E-01 | 264.460 |
| K | L1 | L3 | 2.71099E-01 | 264.470 |
| K | L2 | L2 | 4.20748E-03 | 273.030 |
| K | L2 | L3 | 1.10012E-01 | 273.040 |
| K | L3 | L3 | 6.32008E-02 | 273.050 |
| Nitrogen | | | | |
| *Subshells* | | | *Probability* | *Energy (eV)* |
| K | L1 | L1 | 2.65388E-01 | 358.650 |
| K | L1 | L2 | 1.29999E-01 | 370.250 |
| K | L1 | L3 | 2.58276E-01 | 370.270 |
| K | L2 | L2 | 8.15943E-03 | 381.850 |
| K | L2 | L3 | 2.12711E-01 | 381.870 |
| K | L3 | L3 | 1.22190E-01 | 381.890 |
| Oxygen | | | | |
| *Subshells* | | | *Probability* | *Energy (eV)* |
| K | L1 | L1 | 1.78644E-01 | 478.820 |
| K | L1 | L2 | 1.16224E-01 | 493.860 |
| K | L1 | L3 | 2.30418E-01 | 493.900 |
| K | L2 | L2 | 1.10822E-02 | 508.900 |
| K | L2 | L3 | 2.91115E-01 | 508.940 |
| K | L3 | L3 | 1.66809E-01 | 508.980 |

## 2.2 Biological matter modeling: from water to DNA

In its current version, *TILDA-V* describes the biological components (water and DNA) by means of molecular wave functions within the quantum mechanical framework. For water, we followed the SCF-LCAO (*self-consistent field - linear combination of atomic orbitals*) approach reported by Moccia [14], who described the water molecule by means of single-center wave functions, all centered at a common origin (the oxygen atom). The latter refer to the equilibrium configurations calculated within the self-consistent field method and agree very well with the experimental geometrical and energetic properties of the water molecule. The ten bound electrons of the water target molecule are then distributed among five molecular wave functions corresponding to the five molecular orbitals denoted $1b_1$, $3a_1$, $1b_2$, $2a_1$, and $1a_1$. Each of them is expressed as

$$\upsilon_j(\mathbf{r}) = \sum_{k=1}^{N_{at}(j)} a_{jk} \cdot \Phi^{\xi_{jk}}_{n_{jk}l_{jk}m_{jk}}(\mathbf{r}), \tag{4}$$

with

$$\Phi^{\xi_{jk}}_{n_{jk}l_{jk}m_{jk}}(\mathbf{r}) = R^{\xi_{jk}}_{n_{jk}}(r) \cdot S_{l_{jk}m_{jk}}(\hat{r}), \tag{5}$$

where the radial part $R^{\xi_{jk}}_{n_{jk}}(r)$ is given by

$$R^{\xi_{jk}}_{n_{jk}}(r) = \frac{(2\xi_{jk})^{n_{jk}+1/2}}{\sqrt{(2n_{jk})!}} r^{n_{jk}-1} e^{-\xi_{jk}r}, \tag{6}$$

the angular part $S_{l_{jk}m_{jk}}(\hat{r})$ (where $\hat{r}$ refers to the solid angle) being expressed by means of spherical harmonics in their real form that may be easily rewritten and expressed in terms of complex spherical harmonics as

$$\begin{cases} \text{if } m_{jk} \neq 0: \quad S_{l_{jk}m_{jk}}(\hat{r}) = \left(\frac{m_{jk}}{2|m_{jk}|}\right)^{1/2} \\ \left\{ Y_{l_{jk}-|m_{jk}|}(\hat{r}) + (-1)^{m_{jk}} \left(\frac{m_{jk}}{|m_{jk}|}\right) Y_{l_{jk}|m_{jk}|}(\hat{r}) \right\}, \\ \text{if } m_{jk} = 0: \quad S_{l_{jk}0}(\hat{r}) = Y_{l_{jk}0}(\hat{r}). \end{cases} \tag{7}$$

In equation (4), $N_{at}(j)$ is the number of Slater functions used in the development of the $j$th molecular orbital and $a_{jk}$ is the weight of each real atomic component $\Phi^{\xi_{jk}}_{n_{jk}l_{jk}m_{jk}}(\mathbf{r})$ (more details can be found in Ref. [14] where all the necessary coefficients and quantum numbers are reported).

Regarding DNA, we recently proposed in reference [15] an ab initio approach to express the molecular wave function of each DNA component at the RHF/3-21G level [16] with the GAUSSIAN09 software. In this context, each

**Table 1.** Continued.

| Phosphorus | | | | |
|---|---|---|---|---|
| *Subshells* | | | *Probability* | *Energy (eV)* |
| K | L1 | L1 | 7.12845E-02 | 1756.10 |
| K | L1 | L2 | 7.70090E-02 | 1804.11 |
| K | L1 | L3 | 1.49534E-01 | 1805.07 |
| K | L1 | M1 | 1.42971E-02 | 1926.04 |
| K | L1 | M2 | 3.09277E-03 | 1934.87 |
| K | L1 | M3 | 6.00170E-03 | 1934.92 |
| K | L2 | L2 | 1.35789E-02 | 1852.12 |
| K | L2 | L3 | 3.44468E-01 | 1853.08 |
| K | L2 | M1 | 6.87552E-03 | 1974.05 |
| K | L2 | M2 | 1.05204E-03 | 1982.88 |
| K | L2 | M3 | 1.25152E-02 | 1982.93 |
| K | L3 | L3 | 1.96055E-01 | 1854.04 |
| K | L3 | M1 | 1.33713E-02 | 1975.01 |
| K | L3 | M2 | 1.25043E-02 | 1983.84 |
| K | L3 | M3 | 1.43892E-02 | 1983.89 |
| K | M1 | M1 | 7.12833E-04 | 2095.98 |
| K | M1 | M2 | 2.75938E-04 | 2104.81 |
| K | M1 | M3 | 5.34626E-04 | 2104.86 |
| K | M2 | M2 | 1.72459E-05 | 2113.64 |
| K | M2 | M3 | 3.67923E-04 | 2113.69 |
| K | M3 | M3 | 2.12700E-04 | 2113.74 |
| L1 (2*s*) | L2 | M1 | 2.31157E-01 | 30.8000 |
| L1 (2*s*) | L2 | M2 | 4.82015E-02 | 39.6300 |
| L1 (2*s*) | L2 | M3 | 4.87713E-02 | 39.6800 |
| L1 (2*s*) | L3 | M1 | 4.55856E-01 | 31.7600 |
| L1 (2*s*) | L3 | M2 | 4.78317E-02 | 40.5900 |
| L1 (2*s*) | L3 | M3 | 1.37702E-01 | 40.6400 |
| L1 (2*s*) | M1 | M1 | 9.19772E-03 | 152.730 |
| L1 (2*s*) | M1 | M2 | 6.89081E-03 | 161.560 |
| L1 (2*s*) | M1 | M3 | 1.36935E-02 | 161.610 |
| L1 (2*s*) | M2 | M2 | 8.43928E-05 | 170.390 |
| L1 (2*s*) | M2 | M3 | 2.67913E-06 | 170.440 |
| L1 (2*s*) | M3 | M3 | 1.74150E-04 | 170.490 |
| L2 (2*p*) | M1 | M1 | 3.84224E-02 | 104.720 |
| L2 (2*p*) | M1 | M2 | 4.09857E-01 | 113.550 |
| L2 (2*p*) | M1 | M3 | 2.66610E-02 | 113.600 |
| L2 (2*p*) | M2 | M2 | 1.11541E-01 | 122.380 |
| L2 (2*p*) | M2 | M3 | 4.01870E-01 | 122.430 |
| L2 (2*p*) | M3 | M3 | 1.15410E-02 | 122.480 |
| L3 (2*p*) | M1 | M1 | 3.74626E-02 | 103.760 |
| L3 (2*p*) | M1 | M2 | 1.31656E-02 | 112.590 |
| L3 (2*p*) | M1 | M3 | 4.23652E-01 | 112.640 |
| L3 (2*p*) | M2 | M2 | 1.74570E-03 | 121.420 |
| L3 (2*p*) | M2 | M3 | 2.10574E-01 | 121.470 |
| L3 (2*p*) | M3 | M3 | 3.13300E-01 | 121.520 |

target is described via $N$ molecular subshell wave functions similar to that reported in equation (4) with $N = 35$, 29, 39, 33 and 48 MOs for adenine, cytosine, guanine, thymine and sugar-phosphate backbone unit, respectively. In each case, the molecular subshell wave function is expressed as a linear combination of atomic wave functions corresponding to the different atomic components, namely, $H_{1s}$, $C_{1s}$, $C_{2s}$, $C_{2p}$, $N_{1s}$, $N_{2s}$, $N_{2p}$, $O_{1s}$, $O_{2s}$, $O_{2p}$, $P_{1s}$, $P_{2s}$, $P_{3s}$, $P_{2p}$, and $P_{3p}$. For each molecular orbital (MO) labeled $j$, the effective number of electrons relative to the atomic component $k$ was derived from a standard Mulliken population analysis and their sum for each occupied MO is very close to 2, since only atomic shells with very small population have been discarded. Besides, the computed ionization energies of the occupied MOs of the biological targets investigated here were scaled so that their calculated Koopmans ionization energy, i.e. the ionization energy of their HOMO, coincides with experimental values available in the literature (for more details, we refer the interested reader to our previous study [15], where all the quantum numbers and coefficients needed for expressing the target molecular wave functions as well as the corresponding ionization energy are reported).

Irrespective of the biomolecular targets investigated, *TILDA-V* is based on a cross section database, which refers to *isolated* molecules and to living matter components in *vapor* state. In this context, the present work clearly differs from existing studies on *condensed* matter (water or DNA), where the energy-loss function of realistic biological components was extracted from experimental data and interpolated for use in cross section calculations (see for example Ref. [17] and the recent series of works by Abril and co-workers [18,19] and Emfietzoglou et al. [20]). However, whether it is for water or DNA, the available data – cross sections as well as macroscopic outcomes like ranges and stopping power – are exclusively measured in vapor phase and comparisons with the liquid homologous have been only rarely reported. A *vapor-based* approach is chosen here in order to check the suitability of our theoretical models, although comparisons with existing condensed model will be made hereafter.

In order to gain insight into the real energy deposit cartography induced by proton impact in biological medium, a typical nucleotide has been considered here, i.e. an equivalent unit of DNA molecule composed of a nucleobase-pair plus two SP groups [21]. To fit the realistic composition of living cells, the nucleobase repartition percentages reported by Tan et al. [22], namely, 58% (A-T) (adenine-thymine base pair) and 42% (C-G) (cytosine-guanine base pair) were considered. Thus, by using the respective molar mass of each DNA component, namely, $M_A = 135.14$ g mol$^{-1}$, $M_T = 126.12$ g mol$^{-1}$, $M_C = 111.11$ g mol$^{-1}$, $M_G = 151.14$ g mol$^{-1}$ and $M_{SP} = 180$ g mol$^{-1}$, the following mass percentages were obtained: A (12.6%), T (11.8%), C (7.5%), G (10.2%) and SP group (57.9%). This description refers to *dry* DNA, which obviously cannot mimic the biological reality, mainly composed of hydrated DNA. Consequently, we considered a biological medium composed of hydrated DNA here simulated by adding 18 molecules per nucleotide, that led to the following revisited mass percentages: A (8.3%), T (7.7%), C (4.9%), G (6.7%), SP group (38.1%) and water (34.3%) as suggested by Birnie et al. [23] who estimated that the total amount of water associated with DNA was of the order of 50 moles per mole of nucleotide, in order to get the expected density of 1.29 g cm$^{-3}$. Additionally, we accounted for the nucleobase internal distribution, namely, 0.58 for adenine and thymine, 0.42 for cytosine and guanine, 2 for the sugar phosphate and 18 for the water.

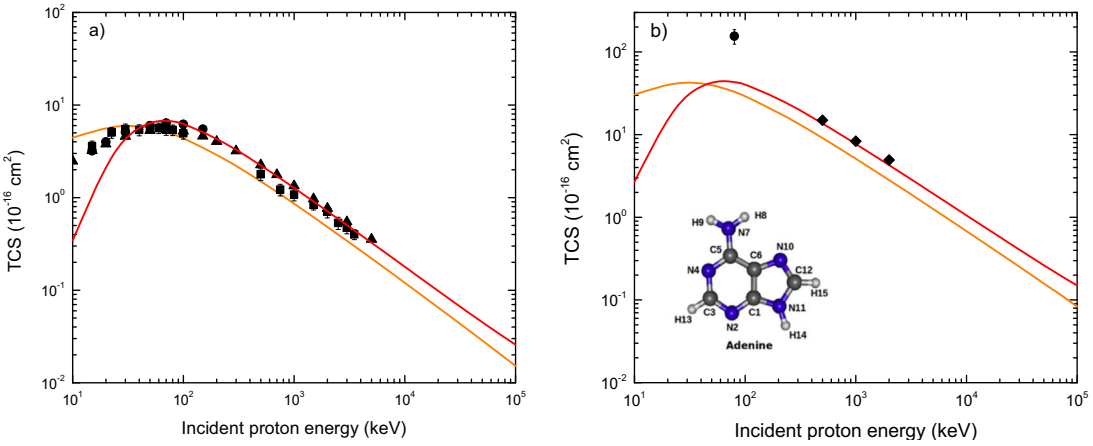


**Fig. 1.** Total cross sections (TCS) for proton-induced ionization in (a) water and (b) adenine, both considered in *vapor* phase. CB1 (orange line) and *prior* CDW-EIS (red line). The experimental data are taken from various sources: (a) Rudd et al. [28] (circles), Bolorizadeh and Rudd [29] (triangles) and Luna et al. [30] (squares); (b) Iriki et al. [25,26] (diamonds) and Tabet et al. [27] (circles).

## 3 Theoretical description of the collisional processes

*TILDA-V* aims at describing the full proton track structure in water and DNA within the energy range 10 keV–100 MeV including the complete slowing-down of all the secondary electrons ($\delta$ rays) down to 7.34 eV. The current version includes a variety of theoretical models independently developed within the quantum mechanical framework for describing the multiple differential and total cross sections of almost all the electron- and proton/hydrogen-induced interactions in water and DNA. An overview of these models is given below. Selected comparisons between theory and experiment are also discussed in order to highlight the consistency as well as the limitations of each approach.

### 3.1 Proton-induced ionization and electron capture

In the current version of *TILDA-V*, the ionization process is described by two different quantum mechanical models: a first one based on a continuum distorted wave-eikonal initial state treatment in its *prior* version (*prior* CDW-EIS) and a second perturbative one developed within the first Born approximation with correct boundary conditions (CB1). In both approaches, the collisional process is modeled within the independent active electron approximation that consists in considering the passive target electrons (those non-ionized) as frozen in their initial orbitals during the collision process. This simplification is generally assumed to overcome the difficulty of taking into account the dynamical correlation between active and passive electrons – as shown by Monti et al. [24] – in particular for large molecules like those investigated here. However, contrary to the CB1 approach which describes the active (ejected) electron as being in bound and continuum states of the target field in the entry and exit channels, respectively, the *prior* CDW-EIS model considers the initial and final distorted wave functions as two-center ones in the sense that the active electron feels the simultaneous presence of the projectile and residual target potentials in the entry and exit channels at all distances between aggregates. Figures 1a and 1b show the total ionization cross sections resulting from both theories for water and the adenine nucleobase.

Figure 1a shows that the present quantum mechanical predictions in terms of total cross sections (TCS) are in close agreement with experiment over the entire energy range covered by the simulation, even considering the well-known underestimation of the *prior* CDW-EIS model below 50 keV incident energy, as well as the overestimation of the CB1 approach at very low energy ($E_{inc} < 20$ keV). Regarding the DNA adenine nucleobase (Fig. 1b), we note that the present theoretical predictions – and more particularly those provided by the *prior* CDW-EIS model – satisfactorily reproduce the recent experimental data of Iriki et al. [25,26], whereas the data reported by Tabet et al. [27] at 80 keV show large discrepancies with our results by a factor of ∼2–5.

Similarly to the ionization process, the single electron capture reaction is described in *TILDA-V* within the independent electron model approach, which considers the passive electrons (the target electrons not captured during the reaction) as frozen in their initial molecular orbital. The multi-electronic problem is reduced to a mono-electronic one involving three effective bodies, namely the projectile, the active electron and the residual target. Only the active electron that is captured during the process of interest is considered.

In *TILDA-V*, the electron capture total cross sections are computed within the distorted wave model by using two different approaches, i.e. the continuum distorted wave (*prior* CDW) [31,32] and the continuum distorted wave-eikonal initial state (*prior* CDW-EIS) models [33,34]. Figure 2 displays a comparison in terms of total cross sections for water and DNA between the theoretical predictions and existing experimental data.

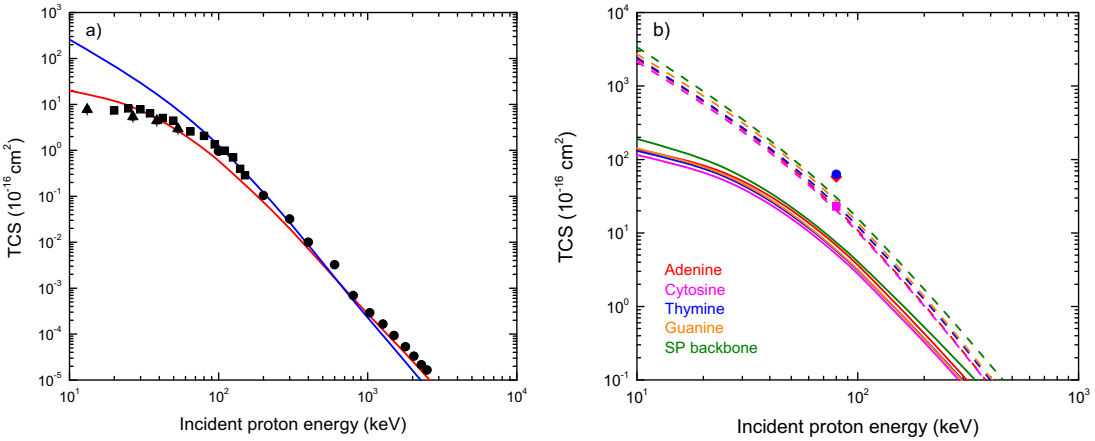


**Fig. 2.** Total cross sections (TCS) for proton-induced capture in (a) water and (b) DNA components in *vapor* phase. Panel (a): *prior* CDW-EIS (red line) and *prior* CDW (blue line); panel (b): *prior* CDW-EIS (solid lines) and *prior* CDW (dashed lines) cross sections. The experimental data are taken from various sources: (a) Dagnac et al. [36] (triangles), Gobet et al. [37] (squares) and Toburen et al. [38] (circles); (b) Tabet et al. [27] (symbols).

For water (Fig. 2a), we observe that the *prior* CDW-EIS approach exhibits a better agreement than the *prior* CDW model, which shows a large overestimation of the experimental total cross sections for proton energies lower than about 100 keV. For DNA, Figure 2b shows that the data reported by Tabet et al. [27] at 80 keV depart from our predictions by about one order of magnitude, a tendency recently confirmed by Privett and Morales using the electron nuclear dynamics (END) framework [35].

### 3.2 Neutral-hydrogen-induced ionization and electron capture

Despite their importance, cross section measurements for water ionization by neutral-hydrogen impact remain extremely rare. Thus, to overcome this limitation, the majority of the existing Monte Carlo codes resort to semi-empirical models among which we distinguish the approach suggested by Dingfelder et al. [17] who used the same secondary-electron spectrum for proton and neutral-hydrogen impact as a starting point but slightly modified by a scaling function that depends only on the incident particle energy and not on the energy transfer. Based on the data of Bolorizadeh and Rudd [39] and those of Toburen and co-workers [38], this scaling function was assumed to be higher than unity at low incident energies and lower than unity for higher energies, in view of the screening of the nuclear charge by the bound electron in hydrogen.

*TILDA-V* aims at going beyond this empirical approach by using the above-cited quantum mechanical models (CB1 and *prior* CDW-EIS). A graphical representation of total cross sections is shown in Figure 3.

Regarding the hydrogen-induced electron capture process, which leads to a negative $H^-$ ion formation, let us note that it has been neglected owing to its very low probability of occurrence. Indeed, in a recent work, Abicht et al. [9] reported experimental and calculated cross sections for various projectile charge transfer processes in water *vapor* and clearly showed that the cross sections for the negative ion $H^-$ production were at least one order of magnitude lower than those corresponding to the hydrogen-induced electron loss process. Under these conditions, this process was neglected and negative ions were discarded in the simulations.

### 3.3 Excitation

Due to the scarcity of experimental data for modeling the excitation process, MCTS codes developed in the last decades are mainly based on the semi-empirical approach proposed by Miller and Green [41], which assumes a velocity scaling of the electron-induced excitation cross sections together with extensions towards lower proton energies (see for example Ref. [42]). In their model, the authors reported a large set of fitting parameters for simulating the proton-induced excitation cross sections for 28 excited states of the water molecule. In *TILDA-V*, we have adopted an extension of this model described by Dingfelder et al. [17], who suggested a slightly modified set of parameters so that the semi-empirical approach agrees with the 1st Born approximation predictions toward the high-energy limit. For DNA components, a similar procedure of velocity scaling of electron-induced excitation cross sections was followed. Experimental total cross sections of electron-induced excitation of DNA components (essentially on thymine; see below the section dedicated to electron-induced excitation cross sections) were used to extrapolate the fitting parameters ($\alpha$, $\beta$, $\Omega$ and $K$) needed in the semi-empirical formula suggested by Miller and Green [41] for modeling the *proton*-induced excitation. Thus, we used in *TILDA-V* the analytical expression

$$\sigma_{exc}\left(E_{inc}\right) = \frac{(Za)^{\Omega}\left(E_{inc} - W\right)^{\upsilon}}{J^{\Omega+\upsilon} + E_{inc}^{\Omega+\upsilon}}, \tag{8}$$

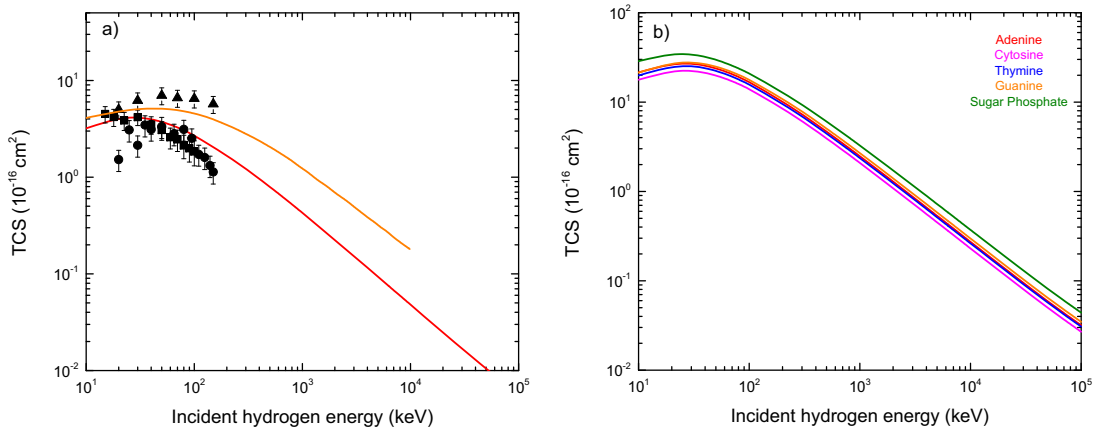


**Fig. 3.** Total cross sections (TCS) for hydrogen atom-induced ionization in (a) water and (b) DNA in *vapor* phase. Panel (a) *prior* CDW-EIS calculations (red line) compared with the semi-empirical predictions of Dingfelder et al. [17] model (orange line). The experimental data are taken from: Luna et al. [30] (squares), Bolorizadeh and Rudd [39] (triangles) and Gobet et al. [40] (circles). (b) *Prior* CDW-EIS calculations.

where $E_{inc}$ designates the impact energy, $Z$ is the number of target electrons and $W$ is an adjustable value of the excitation threshold (here, we used $W = 4$ eV).

In equation (8), the parameter $J$ is given by

$$J = C_2 \frac{M_p}{m_e} W \left(\frac{a\beta + \Omega}{\Omega}\right)^{1/\beta} \left(\frac{\Omega}{\upsilon}\right)^{1/(\Omega+\upsilon)}, \quad (9)$$

where $M_p$ and $m_e$ refer to the proton and the electron mass, respectively, and

$$a = C_2 \frac{M_p}{m_e} \frac{W}{Z} \left[\frac{C_1 \tilde{K}}{W^2} \left(\frac{\upsilon + \Omega}{\upsilon}\right) \left(\frac{\alpha\beta}{\alpha\beta + \Omega}\right)^{\alpha}\right]^{1/\Omega}, \quad (10)$$

with $C_1 = 4$, $C_2 = 0.25$, $\upsilon = 1$ and $\Omega \approx 1$ as suggested by Miller and Green [41]. The coefficient $\tilde{K}$ was computed from the parameter $K$ as $\tilde{K} = Kq_0$, where $q_0$ is a constant value equal to 651.4 [43]. The current values – deduced from those obtained for the thymine ($\alpha = 3.8$, $\beta = 2$, $\Omega = 0.7236$, $K = 0.2985$ and $W = 4$ eV) – are reported in Table 2.

Besides, contrary to Dingfelder et al. [17], who neglected the *neutral-hydrogen*-induced excitation process in view of lack of experimental or theoretical support, *TILDA-V* follows the approach of Uehara et al. [42] who assumed that in water, the neutral-hydrogen cross section could be expressed by the same analytical expression as used for protons (see Eqs. (8)–(10)), provided one of the fitting parameters is changed, namely, the parameter $a$ equal to 3/4 of the proton value [41]. The authors cautioned that the resulting cross section should be considered rough estimates in the absence of experimental or theoretical data. Similarly, the neutral-hydrogen total excitation cross section on DNA components has been computed by using the proton-induced excitation cross section formula reported in equation (8) with the same coefficients used for protons, except for the parameter $a$ which has been rescaled by a factor of 3/4.

**Table 2.** Fitting parameters for the total cross sections of *proton*- and *neutral-hydrogen*-induced excitation of DNA.

| | $a$ ($H^+$) | $a$ ($H^0$) | $J$ | $Z$ |
|---|---|---|---|---|
| Adenine | 8024.02 | 6018.02 | 5161.65 | 70 |
| Cytosine | 7464.75 | 5598.56 | 5161.65 | 58 |
| Guanine | 8364.37 | 6273.28 | 5161.65 | 78 |
| Thymine | 7844.74 | 5883.55 | 5161.65 | 66 |
| Sugar phosphate | 9053.44 | 6790.08 | 5161.65 | 96 |

Figure 4a displays the total excitation cross section (red line) together with the contribution of the five excited states included in the semi-empirical approach of Dingfelder et al. [17], namely, the $\tilde{A}^1B_1$, the $\tilde{B}^1A_1$, the Rydberg A+B, the Rydberg C+D and the diffuse bands, while Figure 4b reports the total cross sections obtained for the various DNA components investigated here.

### 3.4 Proton- and hydrogen-induced elastic scattering

The proton-induced elastic scattering process is treated here within the classical mechanical framework, where the singly differential cross sections (SDCS) are given by the well-known relation

$$\frac{d\sigma}{d\Omega} = -\frac{p}{\sin\theta} \cdot \frac{dp}{d\theta}, \quad (11)$$

where $p$ refers to the impact parameter, i.e. the normal distance between the proton track and the virtual line crossing the center-of-mass (CM) of the system, and $\theta$ denotes the scattering angle within the CM referential defined by

$$\theta = \pi - 2\int_{r_{\min}}^{\infty} \frac{p}{r^2\sqrt{1 - V(r)/E_{inc}^{CM} - p^2/r^2}} dr, \quad (12)$$

with $r_{\min}$ is the distance of closest approach and $E_{inc}^{CM}$ is the incident particle energy in the center-of-mass system. This approach is commonly used in the existing MC codes

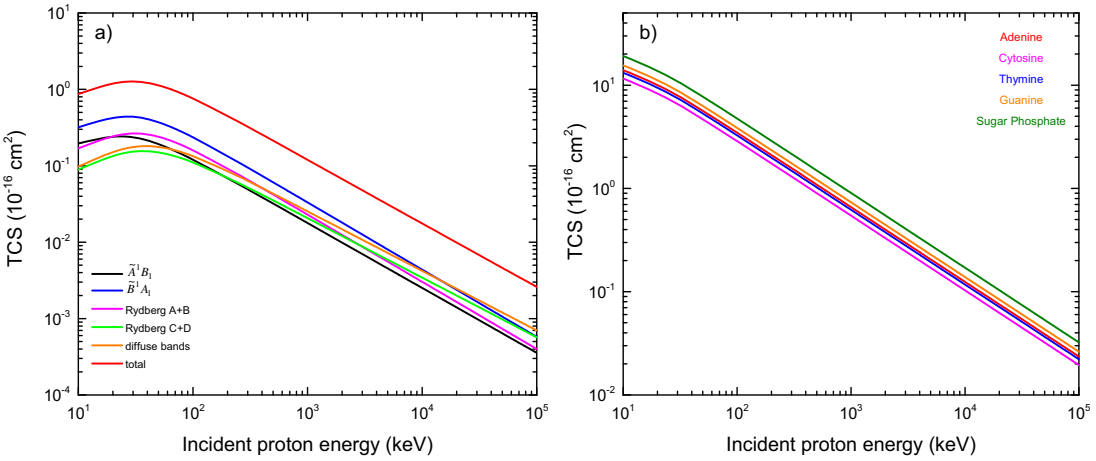


**Fig. 4.** Total excitation cross sections for proton in water *vapor* (panel a) and DNA (panel b).

(see for example Ref. [44]). Contrary to usual studies, where the interaction potential $V(r)$ is approximated by a Coulomb potential described within the Thomas-Fermi model, ab initio potentials numerically computed from the respective target wave function for both water and DNA were utilized here. Total cross sections are obtained by numerical integrations of the SDCS over the scattering solid angle by using a cut-off angle $\theta_{cut}$ in order to reduce the divergence due to the high SDCS at low scattering angles.

Following the suggestion of Endo et al. [45], who analyzed the theoretical calculations reported by Krstic and Schultz [46] for the $H^0 + H_2$ and the $H^+ + H_2$ systems, the hydrogen vs. proton cross section ratio was fitted to

$$\frac{\sigma_{H^0}}{\sigma_{H^+}} = 1 + 0.0224 \log(E_{inc}) + 0.01285 * \log(E_{inc})^2, \quad (13)$$

which leads to a ratio close to unity within the incident energy range considered here.

### 3.5 Secondary electron tracking

All the secondary particles emitted along the various ionizing processes (ionization, electron loss) are followed step-by-step with a MC code, called *EPOTRAN* (an acronym for Electron and Positron Transport in *liquid* and *vapor* water) [47], which presents the particularity of being exclusively based on theoretical cross sections calculated within the quantum mechanical framework except for the excitation process (for more details, see Ref. [48]). More precisely, the ionization process is described within the 1st Born approximation by using a similar partial-wave expansion formalism as reported above, whereas the electron-induced excitation is semi-empirically modeled by using the analytical expression of the total excitation cross section

$$\sigma_{exc}(E_{inc}) = q_0 \frac{K}{W^2} \left(\frac{W}{E_{inc}}\right)^{\Omega} \left[1 - \left(\frac{W}{E_{inc}}\right)^{\beta}\right]^{\alpha}, \quad (14)$$

**Table 3.** Mean excitation energies (in eV) used in *TILDA-V*.

| | Theory | Experiment |
|---|---|---|
| Adenine | 5.45 | 5.8 |
| Cytosine | 5.29 | 5.39 |
| Guanine | 5.38 | – |
| Thymine | 5.74 | 5.5 |
| Tetrahydrofuran | – | 7.56 |

where $E_{inc}$ denotes the incident electron energy, $W$ is the excitation energy (here seen as an adjustable parameter), $q_0$ is a constant value equal to 651.4 [43] and $\alpha$, $\beta$, $\Omega$, $K$ are fitting parameters.

Thus, using a least-square fit to the experimental data of Levesque et al. [49], the values obtained for thymine are: $\alpha = 3.8$, $\beta = 2$, $\Omega = 0.7236$, $K = 0.2985$ and $W = 4$ eV. Cross sections for the other DNA components were simply obtained by scaling proportionally to the number of target electrons. This was taken into account via the parameter $K$ ($K = 0.3166$, $K = 0.2623$, $K = 0.3528$, and $K = 0.4342$ for adenine, cytosine, guanine, and sugar phosphate, respectively). Considering the mean excitation threshold, needed to estimate the energy deposit during the electron-induced excitation, either an average energy estimated from the experimental values reported by Michaud et al. [50] was utilized or a theoretical value provided by Fleig et al. [51] from quantum-mechanical, coupled-cluster methods (see Tab. 3). In the absence of data for the sugar phosphate group, the value of 7.56 eV reported by Bremner et al. [52] for the tetrahydrofuran molecule was used; this approximation is often made in simple models of the deoxyribose building block. For the sake of completeness, let us add that due to the energy cut-off used in the *TILDA-V* code for the secondary electron tracking ($E_{th} = 7.34$ eV), the dissociative electron attachment (DEA) process is not taken into account in the excitation channel even while extremely efficient for inducing single and double strand breaks in particular in the very low-energy regime (8–12 eV) (see the works of the Sanche's group, for example Ref. [53]).

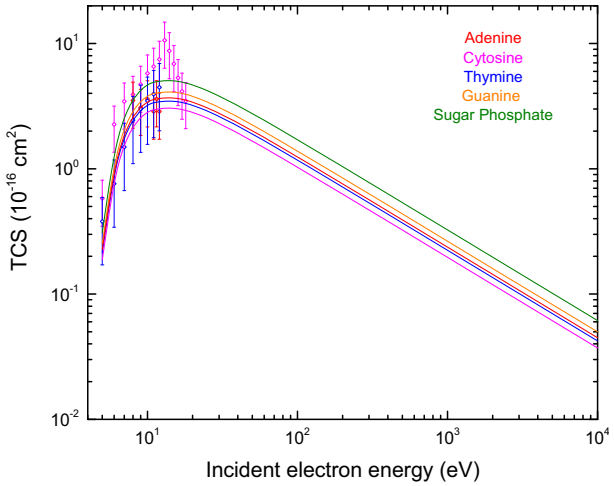


**Fig. 5.** Total excitation cross sections for electron in DNA. Experimental data are taken from several sources (see Michaud et al. [50] for a complete review).

Figure 5 shows the total excitation cross sections of all the DNA components with *TILDA-V*.

Furthermore, the electron tracking is completed by considering the elastic scattering process in water whose description is based on a partial-wave treatment where the interaction potential takes into account a static component – numerically deduced from the molecular target wave functions – as well as exchange and correlation-polarization contributions (see Aouchiche et al. [54]). Work is still in progress for considering the elastic scattering on DNA components.

## 4 Results and discussion

The latest release of *TILDA-V* includes a series of theoretical models and a selection of semi-empirical approaches to palliate the lack of theoretical models for a few processes. Among them is the proton-induced electron loss process – usually called stripping – whose relevance may be crucial in the low-energy regime. An extension of our present theoretical models (Born as well as CDW-EIS) to the description of this projectile ionization process is currently under development.

Further improvement will also focus on describing double ionizing processes, i.e. the double ionization and the ionization transfer (ionization + capture) processes, for protons in water and DNA. The method adopted will be similar to the one proposed by Galassi et al. [55], where the double ionizing processes were treated within an independent-event model, with single particle probabilities calculated as functions of the impact parameter using the CDW-EIS model.

The electron-induced double ionization will be implemented in a near future into the *TILDA-V* database by means of the perturbative model provided by Oubaziz et al. [56]. Those authors reported on a quantum mechanical approach providing a quantitative description of the electron-induced double ionization process on isolated water molecules for impact energies ranging from the target ionization threshold up to ∼10 keV.

Furthermore, the electron tracking will be completed by elastic scattering description in DNA. The chosen approach will be based on a partial-wave treatment similar to that reported above for water, where the interaction potential will account for a static potential numerically deduced from the molecular wave functions as well as exchange and correlation-polarization contributions mentioned above.

Although protons predominantly lose energy via Coulomb interactions with the target electrons, fast protons may also undergo electromagnetic interactions with nuclei, eventually leading to energy and momentum transfers and secondary particles (essentially protons and neutrons and to some extent *alpha*-particles and light fragments such as $d$, $t$ and $^3$He). Accounting for these reactions would be primordial in particular in radiotherapy for predicting the Bragg peak characteristics, whose shape may be modified by such proton-induced nuclear reactions. Possible nuclear reactions – in particular for radiation therapy calculations – have been well documented in the ICRU Report 63 [4]. They include elastic and inelastic collisions with various materials of interest containing oxygen, hydrogen, nitrogen, and other elements. Total nuclear cross sections $Q^{\rm tot}$ are of prime importance for radiotherapeutical treatment planning, since they provide essential information about the decrease in fluence of the primary proton beam, the release of secondary particles and their subsequent transport. Ulmer and co-workers reported a model based on the collective model and the S matrix formalism for providing nuclear cross sections of therapeutic protons [57]. Suitable analytical expressions were provided for both the $Q^{\rm tot}$ cross sections and the energy threshold $E_{\rm th}$, which refers to the energy amount needed to overcome the potential barrier of the impacted target. For proton energies below $E_{\rm th}$ (∼7 MeV for oxygen), nuclear reactions cannot occur. $Q^{\rm tot}$ possesses a maximum value at a resonance energy $E_{\rm res} = 20.12$ MeV, and then decreases exponentially to reach an asymptotic value at ∼100 MeV, typically of about 450 barns for C and 500 barns for O [58]. Because the inelastic cross section is nearly energy independent, the longitudinal pattern of energy deposition is almost independent of depth. Therefore, longitudinal equilibrium develops and the energy of the secondaries is deposited locally (at the reaction point) as a first approximation. Matsuzaki et al. reported a qualitative analysis of the nuclear processes around the Bragg peak (BP) [59]. It was shown that in the region located between the entrance of the proton beam and the BP, the dose due to protons is about 99% of the total absorbed dose, which consists of primary protons without nuclear reactions (≅82%) and p-secondary protons created by proton-induced nuclear reactions (≅18%). Above the BP maximum, the frequency of nuclear reactions sharply decreases, resulting in a lower number of secondary protons. The contribution of the primary protons increases by 6–7% and the ratio of dose due to secondary nuclei is one order of magnitude lower than observed in the previous region. At large distances

**Table 4.** List of theoretical and semi-empirical models implemented in the *standard* version of *TILDA-V*.

| | Process | Model |
|---|---|---|
| Proton | Ionization | *Prior* CDW-EIS |
| | Capture | *Prior* CDW-EIS |
| | Excitation | Semi-empirical approach [41] |
| | Elastic scattering | Classical description |
| Hydrogen | Ionization | *Prior* CDW-EIS |
| | Excitation | Semi-empirical approach [42] |
| | Electron loss | Semi-empirical approach [41] |
| | Elastic scattering | Classical description |

from the BP maximum, the absorbed dose by the secondary protons due to neutron-induced reactions represents ca. 70% of the total absorbed dose, as previously assessed by Paganetti [60] with the GEANT MC package. Therefore, taking into account the nuclear reactions in the full list of proton-induced collisions in biological matter would essentially induce a BP shift upstream, lowering the peak and flattening the entrance region, especially at high proton energies. *TILDA-V* users interested in proton therapy modeling would need to include nuclear models such as the analytical ones proposed by Ulmer et al. into the simulations.

In this context, the *standard* version of *TILDA-V* is based on: (i) CDW-EIS calculations for describing all the ionizing processes induced by both proton and neutral-hydrogen; (ii) the semi-empirical approach proposed by Miller and Green [41] for treating the proton-induced excitation and (iii) the extrapolation suggested by Uehara et al. [42] for describing the neutral-hydrogen induced excitation and electron loss processes (see Tab. 4).

Figure 6 shows the electronic stopping power for protons in water as calculated by the standard version of *TILDA-V*. To do that, one million histories ($N = 10^6$) of *stationary* projectiles (both protons and neutral-hydrogen) were simulated, along which we scored all the inelastic events induced by the *primary particle*. The stopping power (SP) – expressed in keV/$\mu$m – is then defined as the ratio $E_{tot}/L$, where $E_{tot}$ refers to the total amount of energy released by the heavy charged particle of constant energy $E$ while $L$ denotes the ion track length. Thus, from a statistical point of view, the stopping power also provided by *TILDA-V* may be written by

$$SP = \frac{E_{tot}}{L} = \frac{E_{tot}^{\mathrm{H}^+} + E_{tot}^{\mathrm{H}^0}}{L} = \frac{n_{\mathrm{H}^+}\bar{E}^{\mathrm{H}^+} + n_{\mathrm{H}^0}\bar{E}^{\mathrm{H}^0}}{L \cong N\bar{\lambda}}, \quad (15)$$

where $n_{\mathrm{H}^+}$ and $n_{\mathrm{H}^0}$ refer to the scored number of proton- and hydrogen-induced collisions, respectively.

$\bar{E}^{\mathrm{H}^+}$ and $\bar{E}^{\mathrm{H}^0}$ denote the mean energy transfer associated to the corresponding interaction and are expressed by $\bar{E}^{\mathrm{H}^+} = \sum_{j=1}^{3} \bar{E}_j \frac{\sigma_j}{\sigma_{tot}}$ and $\bar{E}^{\mathrm{H}^0} = \sum_{k=1}^{3} \bar{E}_k \frac{\sigma_k}{\sigma_{tot}}$, where $j$ and $k$ (both varying from 1 to 3, see Tab. 4) represent the various interaction types induced by protons and hydrogen atoms, respectively. $\sigma_j$ and $\sigma_k$ are the corresponding cross sections with $\sigma_{tot} = \sigma_j + \sigma_k$.

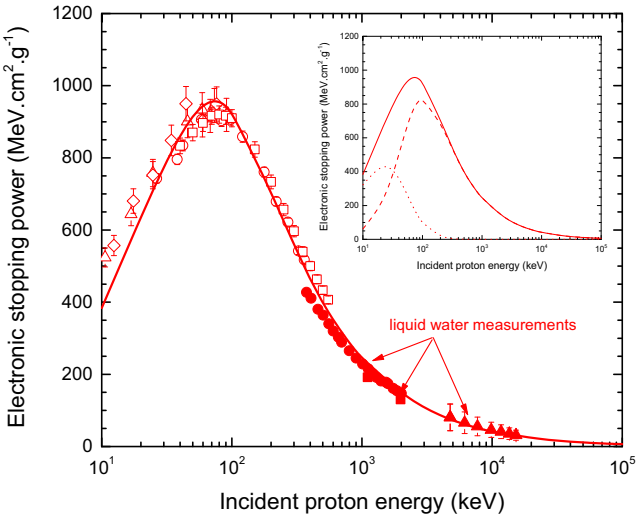


**Fig. 6.** Electronic stopping power (expressed in MeV cm$^2$ g$^{-1}$) as provided by the *standard* version of *TILDA-V* in water. Experimental data are taken from various sources and include measurements in water *vapor* (open symbols: red squares: Reynolds et al. [61], red triangles: Phillips [62], red circles: Mitterschiffthaler and Bauer [63] and red diamonds: Baek et al. [64]), as well as the recent measurements in *liquid* water (solid symbols) provided by Shimizu et al. [65] (squares and circles) and by Siiskonen et al. [66] (triangles). Inset: total stopping power in water *vapor* (red solid line), $H^+$ contribution (red dashed line), and $H^0$ contribution (red dotted line) as provided by *TILDA-V*.

Thus, the stopping power may be written as

$$\begin{aligned} SP &= \frac{1}{\bar{\lambda}\sigma_{tot}} \left[ \frac{n_{\mathrm{H}^+}}{N} \sum_j \bar{E}_j\sigma_j + \frac{n_{\mathrm{H}^0}}{N} \sum_k \bar{E}_k\sigma_k \right] \\ &= n \left[ \frac{n_{\mathrm{H}^+}}{N} \sum_j \bar{E}_j\sigma_j + \frac{n_{\mathrm{H}^0}}{N} \sum_k \bar{E}_k\sigma_k \right] \\ &= n \left[ f_{\mathrm{H}^+} \sum_j \bar{E}_j\sigma_j + f_{\mathrm{H}^0} \sum_k \bar{E}_k\sigma_k \right], \end{aligned} \quad (16)$$

where $f_{\mathrm{H}^+} = n_{\mathrm{H}^+}/N$ and $f_{\mathrm{H}^0} = n_{\mathrm{H}^0}/N$ refer to the equilibrium charge fractions for protons and neutral-hydrogen, respectively. Let us add that in equation (16), $n$ denotes the number of target molecules per volume unit as defined in Section 2.1, i.e. $n = \rho N_A/A_{mol}$, with $\bar{\lambda} = 1/(n\sigma_{tot})$.

Finally, the SP may be related to the usual stopping cross sections (SC) as defined in [42] by

$$\begin{aligned} SP &= n \left[ f_{\mathrm{H}^+} \sum_j \bar{E}_j\sigma_j + f_{\mathrm{H}^0} \sum_k \bar{E}_k\sigma_k \right] \\ &= \frac{\rho N_A}{A_{mol}} \left[ f_{\mathrm{H}^+} \sum_j \bar{E}_j\sigma_j + f_{\mathrm{H}^0} \sum_k \bar{E}_k\sigma_k \right] \\ &= \frac{\rho N_A}{A_{mol}} SC. \end{aligned}$$

Thus, for comparison purpose, considering that all the biomolecular targets studied in the current work are treated as *isolated* molecules (water as well as DNA components), the *TILDA-V* predictions were normalized per *mass unit* by using the liquid water density $\rho = 1$ g cm$^{-3}$.

Figure 6 compares the stopping power for protons in water with the *vapor* stopping cross sections of Reynolds et al. [61] (squares; 30–600 keV), the experimental energy loss data reported by Phillips [62] (up-triangles; 10–80 keV), the stopping cross sections of Mitterschiffthaler and Bauer [63] (circles; 25–350 keV), the measurements of Baek et al. [64] (diamonds; 1–100 keV) and the data by Shimizu et al. [65] in *liquid* water (solid up-triangles; 1–2 MeV), and by Siiskonen et al. [66] (solid down-triangles; 4.7–15.2 MeV). Overall, *TILDA-V* predictions reproduce most of the experimental *vapor* data, except in the very low-energy domain ($E_{inc} < 20$ keV), where the current results slightly underestimate the experiment (≈12–15%). This discrepancy stems from the known *prior* CDW-EIS underestimation of the total ionization cross section in the low-energy range, as reported in Figure 1. As a reminder, in *TILDA-V* simulations the protons are followed until their energies become lower than a predefined cut-off of 10 keV. Thus, under "*realistic*" tracking conditions (i.e. tracking until the particles stop in matter), the stopping cross sections would be slightly larger. For increasing impact energies, the energy cut-off has a lesser influence and the agreement with experiments improves significantly. The maximum observed in experiments is well reproduced by our calculations, both in shape and magnitude, with a location at $E_{inc} \approx 75$ keV and an amplitude of ∼955 MeV cm$^2$ g$^{-1}$.

In the inset of Figure 6 referring to the stopping power of protons in water, the proton contribution was distinguished from the neutral hydrogen contribution in order to highlight the role played by each projectile type in the particle slowing down in the water medium. The hydrogen contribution dominates the energy transfers in the very low-energy regime, below ∼30 keV. Above this value, the proton contribution becomes dominant, which is related to the fact that at these impact energies, the initial projectile charge ($Z = 1$) remains unchanged since the proton-induced electron capture is quasi negligible.

In Figure 7, *TILDA-V* predictions are compared to series of theoretical/semi-empirical calculations and MC simulations in terms of stopping power results in *vapor* water for proton energies limited to the 10 keV–1 MeV range. As expected, the divergences between the various models essentially appear for impact proton energies below ∼1 MeV. More precisely, agreement within 5% is achieved between *TILDA-V* results (red line) and the ICRU49 (green line) [3] and SRIM2006 results (black line) [67] over the whole energy range, with in particular a maximum stopping power of ∼930 MeV cm$^2$ g$^{-1}$ at $E_{inc} \approx 80$ keV for ICRU49 and ∼916 MeV cm$^2$ g$^{-1}$ at $E_{inc} \approx 80$ keV for SRIM2006 [55]. With regard to Janni's tabulation (dark cyan line) [68], those data are slightly higher than both our results and the ICRU49 and SRIM2006 data, in particular for proton energies

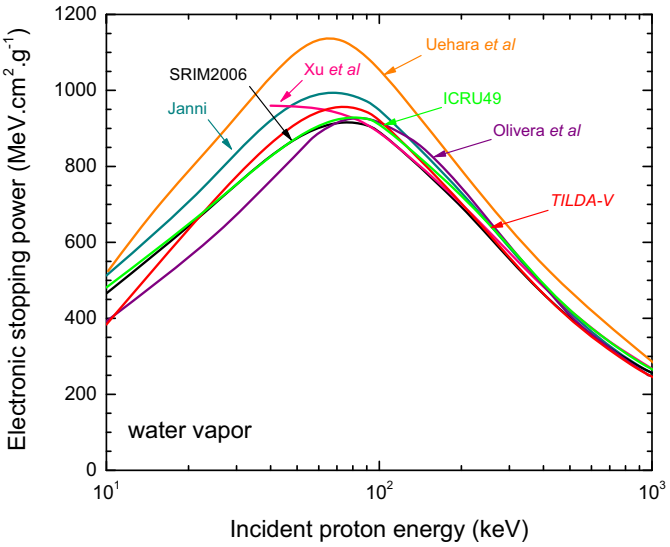


**Fig. 7.** Comparison of our calculations with theoretical data taken from the literature: *TILDA-V* (red line), ICRU49 [3] (green line), Uehara et al. [44] (orange line), SRIM2006 [67] (black line), Janni's tabulation [68] (dark cyan line), Xu et al. [69] (pink line), and Olivera et al. [70] (purple line).

below 100 keV. The calculations by Uehara et al. [44] (orange line) show very large discrepancies over the whole energy range, with an overestimated maximum value of ∼130 MeV cm$^2$ g$^{-1}$ located at lower proton energy ($E_{inc} \approx 60$–70 keV). Uehara and co-workers' calculations of electronic stopping cross sections are based on a compilation of both experimental and semi-empirical cross sections for describing the main processes induced by protons and hydrogen in water. In contrast to the present approach, Uehara et al. calculated the energy transfer during the ionization process by simply accounting for average quantities for both the secondary electron energy and the potential energy locally deposited. Similarly, the calculations of Xu et al. [69] (pink line) performed within a modified local-plasma model are in good agreement with all the results, provided that the proton energy remains larger than 100 keV and, surprisingly, suggest a maximum located at very low proton energy. Slight differences are also observed between the calculations of Olivera et al. [70] within the CDW-EIS framework and the present calculations, in particular for incident energies lower than 100 keV. Part of the discrepancies can be ascribed to the model utilized to calculate the stopping power, where a simple atomic Bragg's rule or a molecular description based on the Bragg's rule was considered (see Olivera et al. [70] and Fainstein et al. [71] for more details), whereas a molecular approach was chosen in our work. However, such refinements have relatively little impact, in particular at the single differential scale and more evidently at the total scale. In a previous study [72], we analyzed the influence of the molecular target representation in the description of the proton-induced ionization and electron capture by testing three approaches: (i) the well-known Bragg's additivity rule which consists

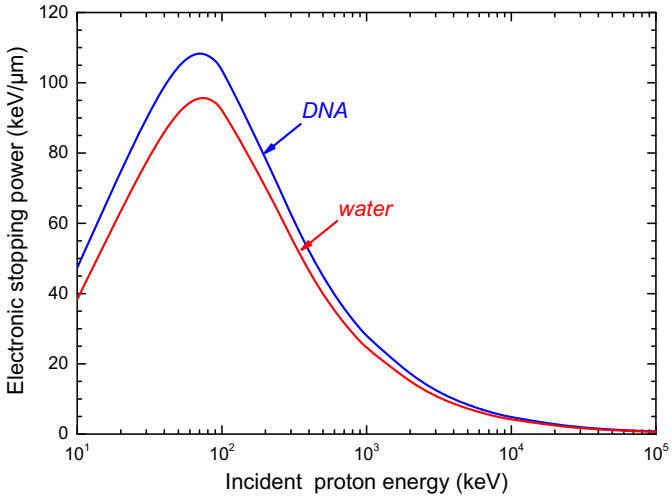


**Fig. 8.** Electronic stopping power in water versus DNA as provided by the *standard* version of *TILDA-V*.

in representing the molecular cross sections as a weighted sum of the cross sections of the different atomic components of the molecule; (ii) the complete neglect of differential overlap (CNDO) approach, where the molecular orbitals are expressed in terms of atomic orbitals of the atomic constituents; and (iii) the MO-LCAO-SCF approach (as provided by Moccia [14]), which describes the populations of the target by means of molecular orbitals constructed from a linear combination of atomic orbitals in a self-consistent field approximation.

Figure 8 represents the electronic stopping power for protons in water versus DNA. The results display a very similar behaviour for both media, with in particular a maximum stopping power located at the same proton energy $E_{inc}$ = 70 keV, showing nevertheless an overestimation of ∼20% in DNA which unambiguously indicate that the approach commonly used in many MC studies – which consists in rescaling the water vapour based track-structure simulations by a realistic density $\rho_{\mathrm{DNA}}/\rho_{\mathrm{H_2O}}$ – is clearly inappropriate for mimicking the biological reality, in particular at the DNA scale and in cellular environment. Besides, let us remind that we used here a DNA density value of 1.29 g cm$^{-3}$ that refers to *hydrated* DNA [23] (see Sect. 2.2), which implies that the above results may slightly differ if *dry* DNA density is used ($\rho = 1.407$ g cm$^{-3}$). Indeed, in a previous study [73], we clearly pointed out that the mean energy deposited by proton tracks in particular biological volumes (typical DNA segment-size cylinder of 2 nm diameter and 2 nm length) was dependent of the DNA density. More precisely, in the low proton-energy regime (<50 keV), we observed an increase of ∼5% for the total energy deposited when the irradiated volume was filled by dry DNA instead of hydrated DNA.

## 5 Conclusions

Whether it is for radiotherapy or radioprotection purposes, a fine understanding of the underlying physics of radiations in living matter is an essential prerequisite of any research at the physics and biology frontier. In this context, Monte Carlo simulations are now accepted as the most suitable and powerful tool for investigating the radio-induced interactions.

We have here detailed our *TILDA-V* code, which refers to a transport code aiming at describing the track-structure of protons and its secondaries in living matter that includes both water and biological species. All the collisions are described at the nanometric scale by means of a large database including total cross sections as well as a variety of differential cross sections ranging from triply to singly differential ones. All the steps of development were validated by theoretical-experimental confrontations in order to select the most appropriate theories for modeling the proton-, hydrogen- and electron-induced interactions with water and DNA targets both described within a molecular approach.

To the best of our knowledge, such a quantum-mechanically based proton transport modeling in a "realistic" biological environment is unique in the dedicated literature.

This well-documented study will serve as a reference work for our forthcoming investigations focused on a water vs. DNA analysis via Monte Carlo simulations of proton histories in complex environment.

We are very grateful to Dr. J.E. Groetz (Lab. Chrono Environment, Univ. Besançon, France) for providing us the FLUKA data and his comments about this work. Sandia National Laboratories is a multi-program laboratory managed and operated by Sandia Corporation, a wholly owned subsidiary of Lockheed Martin Corporation, for the U.S. Department of Energy's National Nuclear Security Administration under contract DE-AC04-94AL85000. This work has been developed as part of the activities planned in the INSERM project (Plan Cancer 2009–2013) called "MICRONAUTE". Finally, J.M. Monti, O.A. Fojón and R.D. Rivarola acknowledge financial support from the Agencia Nacional de Promoción Científica y Tecnológica (Project PICT 2011-2145) and the Consejo Nacional de Investigaciones Científicas y Técnicas (PIP-CONICET 1026/10), both institutions from the República Argentina.

## Author contribution statement

All authors participated in the Monte Carlo simulation development as well as the writing and the revising of the text.

## References

1. H. Nikjoo, S. Uehara, D. Emfietzoglou, F.A. Cucinotta, Radiat. Meas. **41**, 1052 (2006)
2. International Commission on Radiation Units Measurements, ICRU Report 16, ICRU, Washington, DC, USA (1970)

3. International Commission on Radiation Units Measurements, ICRU Report 49, ICRU, Washington, DC, USA (1993)
4. International Commission on Radiation Units Measurements, ICRU Report 63, ICRU, Washington, DC, USA (2000)
5. International Atomic Energy Agency Atomic and Molecular Data for Radiation Therapy and Related Research, IAEA-TECDOC-799, IAEA, Vienna, Austria (1995)
6. W. Friedland, P. Jacob, P. Bernhardt et al., Radiat. Res. **159**, 401 (2003)
7. M.A. Quinto, J.M. Monti, M.E. Galassi, P.F. Weck, O.A. Fojón, J. Hanssen, R.D. Rivarola, C. Champion, J. Phys. Conf. Ser. **583**, 012049 (2015)
8. C. Champion, A. L'Hoir, M.F. Politis, P.D. Fainstein, R.D. Rivarola, A. Chetioui, Radiat. Res. **163**, 222 (2005)
9. F. Abicht, R. Prasad, M. Borghesi, G. Priebe, J. Braenzel, A. Andreev, P.V. Nickles, M. Schnürer, S. Jequier, G. Revet, V. Tikhonchuk, S. Ter-Avetisyan, Appl. Phys. Lett. **103**, 253501 (2013)
10. M. Michaud, P. Cloutier, L. Sanche, Phys. Rev. A **44**, 5624 (1991)
11. J. Meesungnoen, J.P. Jay-Gerin, A. Filali-Mouhim, S. Mankhetkorn, Radiat. Res. **158**, 657 (2002)
12. C. Martin, Ph.D. thesis, Univertity of Toulouse, France, 2003
13. S.T. Perkins, D.E. Cullen, M.H. Chen, J.H. Hubbel, J. Rathkopf, J. Scofield, Tables and Graphs of Atomic Subshell and Relaxation Data Derived from the LLNL Evaluated Atomic Data Library (EADL), $Z = 1$–100, Lawrence Livermore National Laboratory Report, UCRL-50400, **30** (1991)
14. R. Moccia, J. Chem. Phys. **40**, 2186 (1964)
15. M.E. Galassi, C. Champion, P.F. Weck, R.D. Rivarola, O. Fojón, J. Hanssen, Phys. Med. Biol. **57**, 2081 (2012)
16. M.J. Frisch et al., *Gaussian 09, Revision A.02* (Gaussian, Inc., Wallingford, CT, 2009)
17. M. Dingfelder, M. Inokuti, H.G. Paretzke, Radiat. Phys. Chem. **59**, 255 (2000)
18. I. Abril, R. Garcia-Molina, C.D. Denton, I. Kyriakou, D. Emfietzoglou, Radiat. Res. **175**, 247 (2011)
19. P. de Vera, R. Garcia-Molina, I. Abril, Phys. Rev. Lett. **114**, 018101 (2015)
20. D. Emfietzoglou, K. Karava, G. Papamichael, M. Moscovitch, Phys. Med. Biol. **48**, 2355 (2003)
21. J.A. La Verne, S.M. Pimblott, Radiat. Res. **141**, 208 (1995)
22. Z. Tan, Y. Xia, M. Zhao, X. Liu, Nucl. Instrum. Methods B **248**, 1 (2006)
23. G.D. Birnie, D. Rickwood, A. Hell, Biochim. Biophys. Acta **331**, 283 (1973)
24. J.M. Monti, O.A. Fojón, J. Hanssen, R.D. Rivarola, J. Phys. B **42**, 195201 (2009)
25. Y. Iriki, Y. Kikuchi, M. Imai, A. Itoh, Phys. Rev. A **84**, 032704 (2011)
26. Y. Iriki, Y. Kikuchi, M. Imai, A. Itoh, Phys. Rev. A **84**, 052719 (2011)
27. J. Tabet, S. Eden, S. Feil, H. Adboul-Carime, B. Farizon, M. Farizon, S. Ouaskit, T.D. Märk, Phys. Rev. A **82**, 022703 (2010)
28. M.E. Rudd, T.V. Goffe, R.D. DuBois, L.H. Toburen, Phys. Rev. A **31**, 492 (1985)
29. M.A. Bolorizadeh, M.E. Rudd, Phys. Rev. A **33**, 888 (1986)
30. H. Luna, A.L.F. Barros, J.A. Wyer, S.W.J. Scully, J. Lecointre, P.M.Y. Garcia, G.M. Sigaud, A.C.F. Santos, V. Senthil, M.B. Shah, C.J. Latimer, E.C. Montenegro, Phys. Rev. A **75**, 042711 (2007)
31. I.M. Cheshire, Proc. Phys. Soc. **84**, 89 (1964)
32. Dz. Belkic, R. Gayet, A. Salin, Phys. Rep. **56**, 279 (1979)
33. A.E. Martinez, G.R. Deco, R.D. Rivarola, P.D. Fainstein, Nucl. Instrum. Methods B **43**, 24 (1989)
34. P.N. Abufager, A.E. Martínez, R.D. Rivarola, P.D. Fainstein, J. Phys. B **37**, 817 (2004)
35. A.J. Privett, J.A. Morales, Chem. Phys. Lett. **603**, 82 (2014)
36. R. Dagnac, D. Blanc, D.D. Molina, J. Phys. B **3**, 1239 (1970)
37. F. Gobet, B. Farizon, M. Farizon, M.J. Gaillard, Phys. Rev. Lett. **86**, 3751 (2001)
38. L.H. Toburen, M.Y. Nakai, R.A. Langley, Phys. Rev. **171**, 114 (1968)
39. M.A. Bolorizadeh, M.E. Rudd, Phys. Rev. A **33**, 893 (1986)
40. F. Gobet, S. Eden, B. Coupier, J. Tabet, B. Farizon, M. Farizon, M.J. Gaillard, S. Ouaskit, M. Carre, T.D. Märk, Chem. Phys. Lett. **421**, 68 (2006)
41. J.H. Miller, A.E.S. Green, Radiat. Res. **54**, 343 (1973)
42. S. Uehara, L.H. Toburen, W.E. Wilson, D.T. Goodhead, H. Nikjoo, Radiat. Phys. Chem. **59**, 1 (2000)
43. J.J. Olivero, R.W. Stagat, A.E.S. Green, J. Geophys. Res. **77**, 4797 (1972)
44. S. Uehara, L.H. Toburen, H. Nikjoo, Int. J. Radiat. Biol. **77**, 139 (2001)
45. S. Endo, E. Yoshida, H. Nikjoo, M. Hodhi, M. Ishikawa, K. Shizuma, Nucl. Instrum. Methods Phys. Res. B **194**, 123 (2002)
46. P.S. Krstic, R.R. Schultz, Oak Ridge National Laboratory, Oak Ridge, TN, 1998
47. C. Champion, C. Le Loirec, B. Stosic, Int. J. Radiat. Biol. **88**, 62 (2012)
48. C. Champion, Phys. Med. Biol. **48**, 2147 (2003)
49. P.L. Levesque, M. Michaud, W. Cho, L. Sanche, J. Chem. Phys. **122**, 224704 (2005)
50. M. Michaud, M. Bazin, L. Sanche, Int. J. Radiat. Biol. **88**, 15 (2012)
51. T. Fleig, S. Kneht, C. Hättig, J. Phys. Chem. A **111**, 5482 (2007)
52. L.J. Bremner, M.G. Curtis, I.C. Walker, J. Chem. Soc. Faraday Trans. **87**, 1049 (1991)
53. L. Sanche, in *Radical and Radical Ion Reactivity in Nucleic Acid Chemistry*, edited by M.M. Greenberg (John Wiley & Sons, Inc., 2009)
54. H. Aouchiche, C. Champion, D. Oubaziz, Radiat. Phys. Chem. **77**, 107 (2008)
55. M.E. Galassi, P.N. Abufager, A.E. Martinez, R.D. Rivarola, P.D. Fainstein, J. Phys. B **35**, 1727 (2002)
56. D. Oubaziz, M.A. Quinto, C. Champion, Phys. Rev. A **91**, 022703 (2015)
57. W. Ulmer, E.A. Matsinos, J. Nucl. Particle Phys. **2**, 42 (2012)
58. W. Ulmer, Int. J. Cancer Ther. Oncol. **2**, 020211 (2014)
59. Y. Matsuzaki, H. Date, K. Lee Sutherland, Y. Kiyanagi, Radiol. Phys. Technol. **3**, 84 (2010)
60. H. Paganetti, Phys. Med. Biol. **47**, 747 (2002)

61. H.K. Reynolds, D.N.F. Dunbar, W.A. Wenzel, W. Whaling, Phys. Rev. **92**, 742 (1953)
62. J.A. Phillips, Phys. Rev. **90**, 532 (1953)
63. C. Mitterschiffthaler, P. Bauer, Nucl. Instrum. Methods Phys. Res. B **48**, 58 (1990)
64. W.Y. Baek, B. Grosswendt, G. Willems, Radiat. Prot. Dosimetry **122**, 32 (2006)
65. M. Shimizu, M. Kaneda, T. Hayakawa, H. Tsuchida, A. Itoh, Nucl. Instrum. Methods B **267**, 2667 (2009)
66. T. Siiskonen, H. Kettunen, K. Peräjärvi, A. Javanainen, M. Rossi, W.H. Trzaska, J. Turunen, A. Virtanen, Phys. Med. Biol. **56**, 2367 (2011)
67. J.F. Ziegler, J.P. Biersack, U. Littmark, *The Stopping and Range of Ions in Solids* (Pergamon Press, New York, 2003)
68. J.F. Janni, At. Data Nucl. Data Tables **27**, 147 (1982)
69. Y.J. Xu, G.S. Khandelwal, J.W. Wilson, Phys. Rev. A **32**, 629 (1985)
70. G. Olivera, A.E. Martínez, R.D. Rivarola, P.D. Fainstein, Radiat. Res. **144**, 241 (1995)
71. P.D. Fainstein, G.H. Olivera, R.D. Rivarola, Nucl. Instrum. Methods B **107**, 19 (1996)
72. C. Champion, M.E. Galassi, P.F. Weck, O. Fojón, J. Hanssen, R.D. Rivarola, in *Radiation Damage in Biomolecular Systems, Biological and Medical Physics, Biomedical Engineering*, edited by G.G. Gómez-Tejedor, M.C. Fuss (Springer Science, 2012), pp. 263–289
73. C. Champion, M.A. Quinto, J.M. Monti, M.E. Galassi, P.F. Weck, O.A. Fojn, J. Hanssen, R.D. Rivarola, Phys. Med. Biol. **60**, 7805 (2015)